Desalination and Water Treatment
www.deswater.com
doi: 10.5004/dwt.2021.26674

213 (2021) 229–239
February

Enhancement of ciprofloxacin antibiotic removal from aqueous solution using ZnO nanoparticles coated on pistachio shell

Ahmed A. Mohammed[a], Sabreen L. Kareem[b,*]

[a]*Department of Environmental Engineering, College of Engineering, University of Baghdad, Iraq, email: ahmed.abedm@yahoo.com*
[b]*Department of Environmental Planning, College of Physical Planning, University of Kufa, Iraq, email: sabreenl.kareem@uokufa.edu.iq*

Received 29 April 2020; Accepted 14 October 2020

ABSTRACT

In this study, pistachio shell coated with zinc oxide nanoparticles (CPS) were used as powder as a novel adsorbent for elimination of ciprofloxacin (CIP) from simulated wastewater. Functional groups, surface morphology, and surface area of CPS were observed by Fourier transform infrared spectroscope, scanning electron microscope, and surface area analysis, respectively. Effects of significant parameters (pH, particle size, shaking speed, CPS dosage and initial CIP concentration) on CIP adsorption were studied. Langmuir isotherm model was found to fit more than Freundlich model. The maximum uptake of 129.1 mg/g was obtained at pH 7, 0.1 g CPS/100 mL CIP solution, 87 μm particle size, 150 rpm at 25°C. Pseudo-second-order kinetic model was the best fit with high determination coefficient (R^2) and more closely to experimental uptake compared with pseudo-first-order, also the intraparticle diffusion was not the prevailing mechanism. Finally, thermodynamic parameters ($\Delta G°$ and $\Delta H°$) presented that CIP adsorption onto CPS was spontaneous and exothermic in nature. The consequences verified that CPS is found to be an excellent media for CIP elimination from aqueous solution.

Keywords: Adsorption; Ciprofloxacin; Nanoparticles; Coating; Pistachio shell

1. Introduction

Pharmaceutical compounds especially antibiotics are extensively used for diseases treatment or prevention [1]. Antibiotics based on their physical and chemical properties are categorized into several groups, amongst various groups fluoroquinolones (FQs) prescribed for treatment of respiratory infections and bacteria [2]. Ciprofloxacin (CIP), prescribed in the FQ category, compared with other antibiotics exist in high concentration in aquatic environment [3]. Antibiotics usually are not completely metabolized in animal and human bodies and may be incompletely removed from wastewater treatment plants, hence the treated effluents comprise some amounts of antibiotics [4].

The most generally used procedures for antibiotic removal from aqueous solution are adsorption, liquid membrane separation, electro-Fenton oxidation, bioaugmentation, sono-chemical degradation, nanofiltration, and enzymatic complexation [5]. Adsorption, among them, has some benefits such as easy in design, cost effective, operate easily, and toxic material insensitivity. These benefits make the procedure more effective [6]. Porcelanite [7], groundnut [8], Hazelnut [9], Kandira stone [10], CuO nanoparticles [11], multi-walled carbon nanotubes [12], and oat hulls [13] are the most famous media used to treat wastewater from antibiotics, especially ciprofloxacin. Recent research tends to increase the ability of natural waste material as adsorbents and tends to produce significant adsorbents with high efficiency. Thus, synthesis

* Corresponding author.

materials were developed especially by coating natural materials with nanoparticles, which promote the adsorbent features such as surface area, mechanical strength, and adsorption capacity [8]. Nanoparticle-based adsorbent have significant properties such as catalytic potential, high reactivity, and large surface area. The nanoparticle-based adsorbents, used for polluted water treatment, were synthesized from alumina, copper oxide, gold, iron oxide, zinc oxide, stannous oxide, titanium oxide, and some alloys [14]. Pure nanoparticles have some disadvantages such as not cost effective, tendency to agglomerate causing significant reactivity, loss and a drop in pressure in traditional treatment systems in addition to the fact that its separation from aqueous phase needs advanced filtration technology. Therefore, natural adsorbents coated with nanoparticles is an efficient alternative, avoiding the problems of using nanomaterials alone and increasing the efficiency of the main adsorbents to remove contaminants from different sources [15,16]. Zinc oxide (ZnO) nanoparticle (ZnONPs) synthesis cost was low and can be used in various fields [17,18]. Ciprofloxacin (CIP), as a fluoroquinolone antibiotic, is one of the greatest extensively prescribed antibiotics in humans and animals. CIP was proven to be effective in treatment of numerous bacterial infections, for example, bone respiratory and urinary infections. CIP molecular formula is $C_{17}H_{18}FN_3O_3$ and the molecular weight (MW) is 331.346 g/mol as shown in Table 1 [13].

As shown in Fig. 2, CIP molecules exist in two acid dissociation constants at different pH values. The first one (pKa_1) was corresponding to the carboxylic and the other (pKa_2) attributed to N-moiety groups, respectively. At pH values lower than the pKa_1, the amine groups are protonated and hence the CIP+ (cationic form) is dominantly present in the media. However, at pH values higher than pKa_2 carboxyl and N-moiety groups are deprotonated, resulting in CIP- (anionic form) mostly present in the system [13].

In this study, pistachio shell (PIS) coated with ZnO nanoparticles (CPS) were prepared for CIP removal. This new adsorbent was characterized by X-ray diffraction (XRD), scanning electron microscopy (SEM), and Fourier transform infrared (FTIR). Adsorption kinetics, isotherms, thermodynamics, and capacity of the CIP-CPS were tested under different parameters including pH, adsorbent dose, shaking speed, temperature, particle size, contact time, and initial CIP concentrations.

2. Materials and methods

2.1. Synthesis and characterization of PIS and CPS

CPS was prepared as follows:

- PIS shells were locally collected, manually cleaned, washed with purified water for 2–3 h, and then dried by appropriate oven at 105°C for 24 h.
- The dried PIS shells prepared were powdered and sieved. Some PIS prepared amounts were characterized, and the remaining was stored for the nanoparticles surface coating.
- ZnONPs obtained from Xi'an Lyphar Biotech Co., Ltd., China. PIS coating with the ZnONPs was done using an ultrasonic device.
- The ZnONPs were added to acetone (suitable dispersant) in an ultrasonic device for 30 min and then PIS powder prepared above was added in different mass ratio and shaken for 2 h to obtain CPS.
- Finally, the dried CPS was kept in stoppered containers to be used in the necessary experiments.

2.2. Ch-emicals

Powdered CIP, purity: 98%, was obtained from General Company for drugs industry (Samarra, Iraq). CIP stock solution was prepared by dissolving a suitable amount of powdered CIP in 1 L of distilled water. Solution should be prepared daily at the time of experiments due to CIP instability at laboratory conditions. The initial pH values of the solutions were modified by the addition of 0.1 M NaOH or HCl. Point of zero charge of adsorbents (pHpzc) was determined according to the procedure illustrated in the study by Sharma and Neeraj [19].

2.3. Batch experiments

- pH effect in (range 3–9) was tested by adding 50 mg CPS to 50 mg/g CIP solution and in a 250 mL flask and shaken for 2 h in a shaker at 200 rpm.
- CPS dose effect investigated in the range 200–1,000 mg/100 CIP mL on 50 mg/g CIP elimination.
- Shaking speeds effect in range 150, 200, and 250 rpm on CIP adsorption were tested at the best CPS dose and pH obtained from 1 and 2 experiments.
- Particle size influence in the range 194, 122, and 87 μm on CIP removal conducted using 50 mg/g CIP solution at pH 6, 1,000 mg CPS/100 mL solution, 150 rpm, and 2 h shaking time.
- The result of changing shaking time and initial CIP concentration on the removal efficiency conducted using, 1,000 mg CPS/100 mL CIP aqueous solution and CIP concentrations range (30, 40, 50, 60, and 70 ppm) for 2 h, at the optimum tested parameter value obtained from the p1,2,3 and 4 experiments.
- The influence of temperature on CIP elimination was obtained by adjusting solution temperature value (25°C, 30°C, and 35°C) under the best tested parameters value as identified by the earlier tests, and the results were used in thermodynamic study.

Table 1
Chemical structure and physicochemical features of ciprofloxacin

	Molecular formula	Purity	Molecular weight	CAS	pKa_1	pKa_2
Ciprofloxacin	$C_{17}H_{18}FN_3O_3$	≥ 98%	331 g/mol	85721-33-1	6.1	8.7

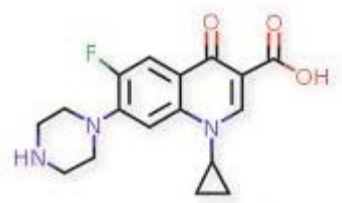

Fig. 1. Chemical structure of CIP [1].

In all experiments, the sample was filtered and tested for CIP concentrations using a (UV/VIS) spectrophotometer (Shimadzu, Japan). For more accuracy, three readings were recorded and the average for them are depended. Equilibrium adsorption capacity (q_e, mg/g) was determined using (Eq. (1)) and the CIP removal efficiency R (%) was calculated using (Eq. (2)) as follows: [18–20]

$$q_e = \frac{\left(C_0 - C_e\right)V}{W} \tag{1}$$

$$R(\%) = \left(\frac{C_0 - C_e}{C_0}\right)100 \tag{2}$$

where C_0 and C_e are the CIP initial and equilibrium concentrations (mg/L), respectively; V is the volume of solution sample (L), and W is the CPS adsorbent mass (g).

3. Results and discussion

3.1. Characterization of materials

In order to verify the purity of ZnO nanoparticles, TEM images in Fig. 3 proved that the average particle size of ZnONP was 50 nm [16]. XRD was tested and the result is shown in Fig. 4a, which shows that 100% of material was ZnO and was found to be in hexagonal structure, also this result was proved by comparing the given material XRD peaks with standard ZnO XRD card, the synthesized ZnO nanoparticles average diameter (d) was calculated using (Eq. (3); Debye–Scherrer formula).

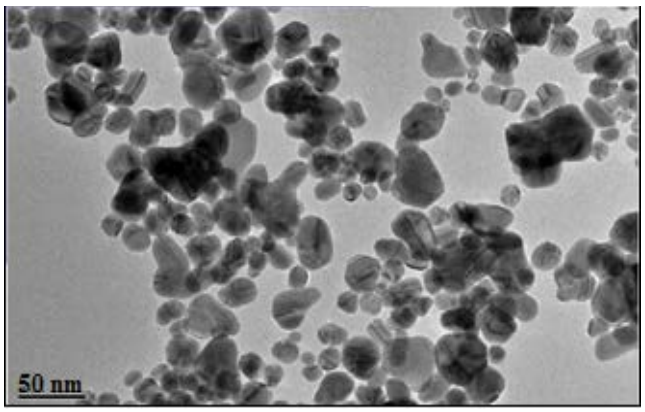

Fig. 3. TEM image of ZnO nanoparticles.

$$d = \frac{0.89\lambda}{b\cos\theta} \tag{3}$$

where d is the diameter of nanoparticle, λ is the X-ray wave length (usually for CuO), 0.89 is the Scherrer's constant, b is FWHM (full width at half maximum, and θ is the Bragg's angle by applying Eq. (3). ZnONP diameter was established to be 20.9 nm [21,22].

Fig. 4 depicts XRD forms of PIS and CPS, respectively. The PIS XRD analysis (Fig. 4b) displays that the PIS main ingredients were cristobalite (97.4%) and periclase (2.6%). XRD analysis of CPS displays the forming of new peaks as seen in Fig. 2c owing to the newly resulted ZnONP layers. However, peak diffraction is observed at position ((2θ)) = 31.7288, 34.3877, 36.2432, 47.5063, 56.5137, and 62.8756, which relate to the reflection from (100), (002), (101), (102), (110), and (103) planes, respectively. These were owing to the ZnO layer (100%) and similarly showed that the shells of the PIS were shielded with pure ZnONP.

ZnONP particle size calculated from the XRD and TEM results was different, owing to overlap of "secondary particles" resulted after the primary particles adhere together by accumulation owing to chemical bonding "soft agglomerates" or by fragile surface forces such as "Van der Waals" or "capillary forces" [21].

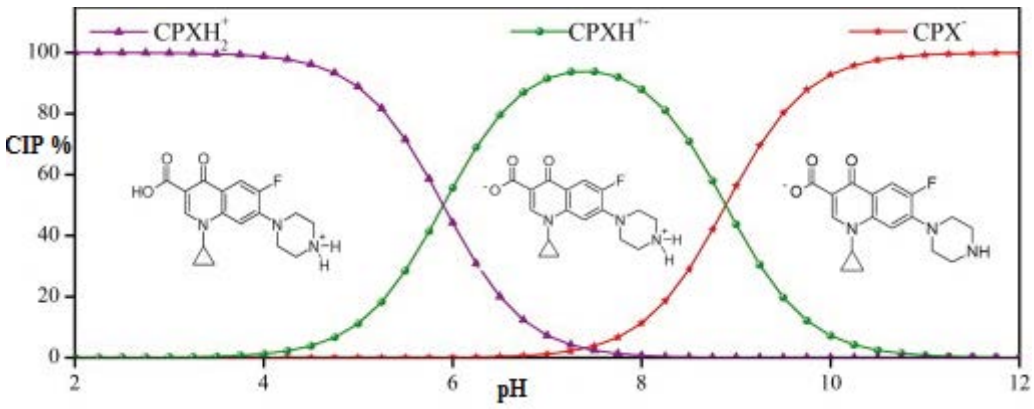

Fig. 2. Speciation of CIP at different pH values [13].

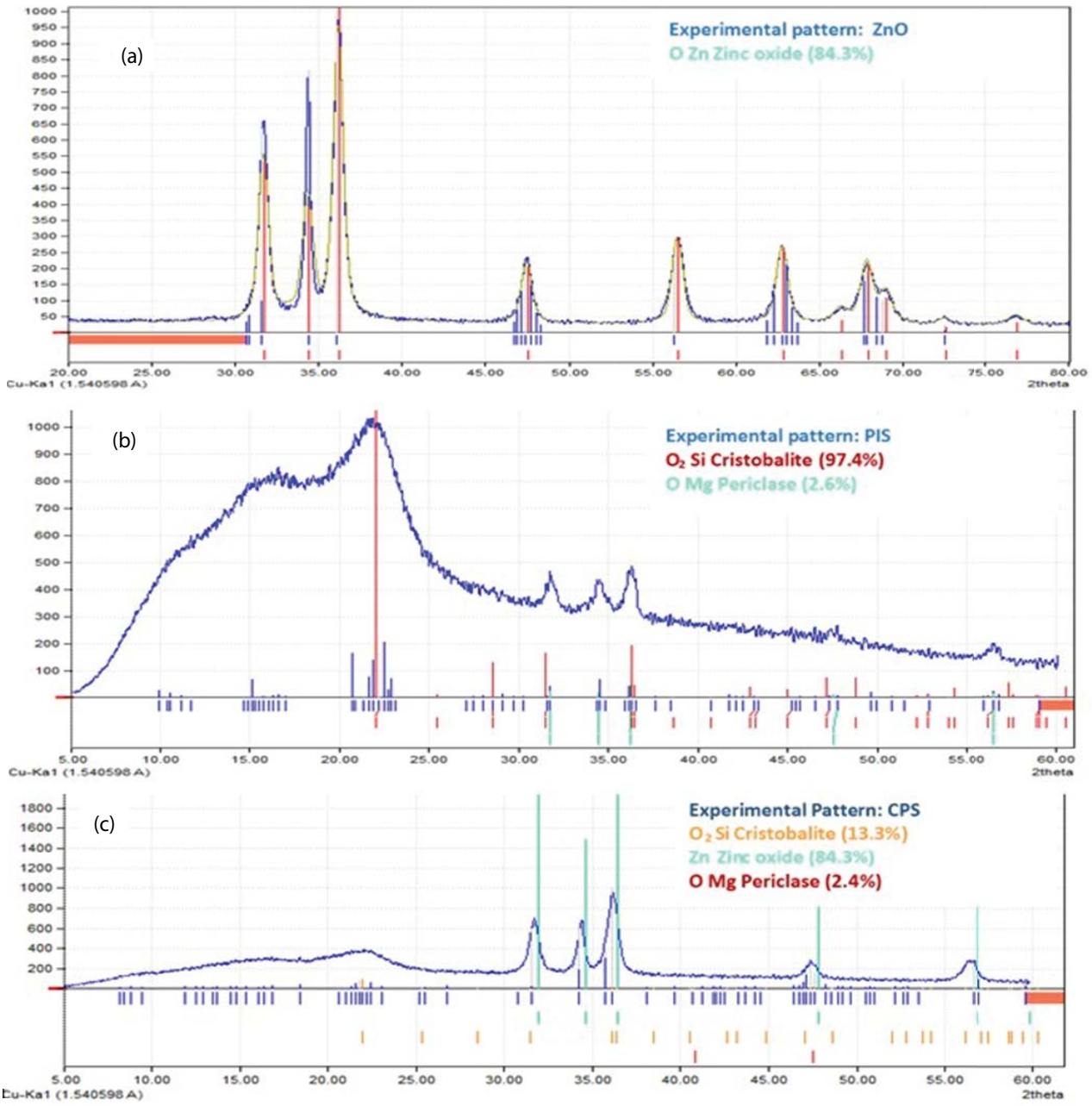

Fig. 4. XRD patterns of (a) ZnO, (b) PIS, and (c) CPS.

SEM images clarify the surface morphology of PIS, ZnO, and CPS before and after CIP adsorption. The representative images are shown in Figs. 5a–d. The surface morphology of natural pistachio shell before preparation of the nano composite was shown in Fig. 5a; this figure shows that the PIS surface was coarse, regular with spherical irregular aggregates. Numerous small pores and cavities were detected making PIS a good supportive surface for ZnONP.

The SEM of the CPS in Fig. 5b indicated that the CPS surface is coarse; also it contains several non-uniform and separated aggregates. So, there are many great ravines and extended grooves in the CPS outer wall. These CPS surface morphological characteristics represented as a positive instant provide a high surface area for CIP molecules sorbing. In this direction, the specific surface area of PIS was determined to be equal to 0.972 m^2/g, which was significantly increased after coating with ZnO nanoparticles to be equal to 4.234 m^2/g. This allows CIP molecules to enter into it and interact with surface functional groups. Comparing Fig. 5b (CPS SEM image before CIP adsorption) with Fig. 5c (CPS SEM image after CIP adsorption), the morphological properties of CPS were significantly altered during the CIP adsorption. The CPS surface becomes brighter and smoother, and several pre-separated

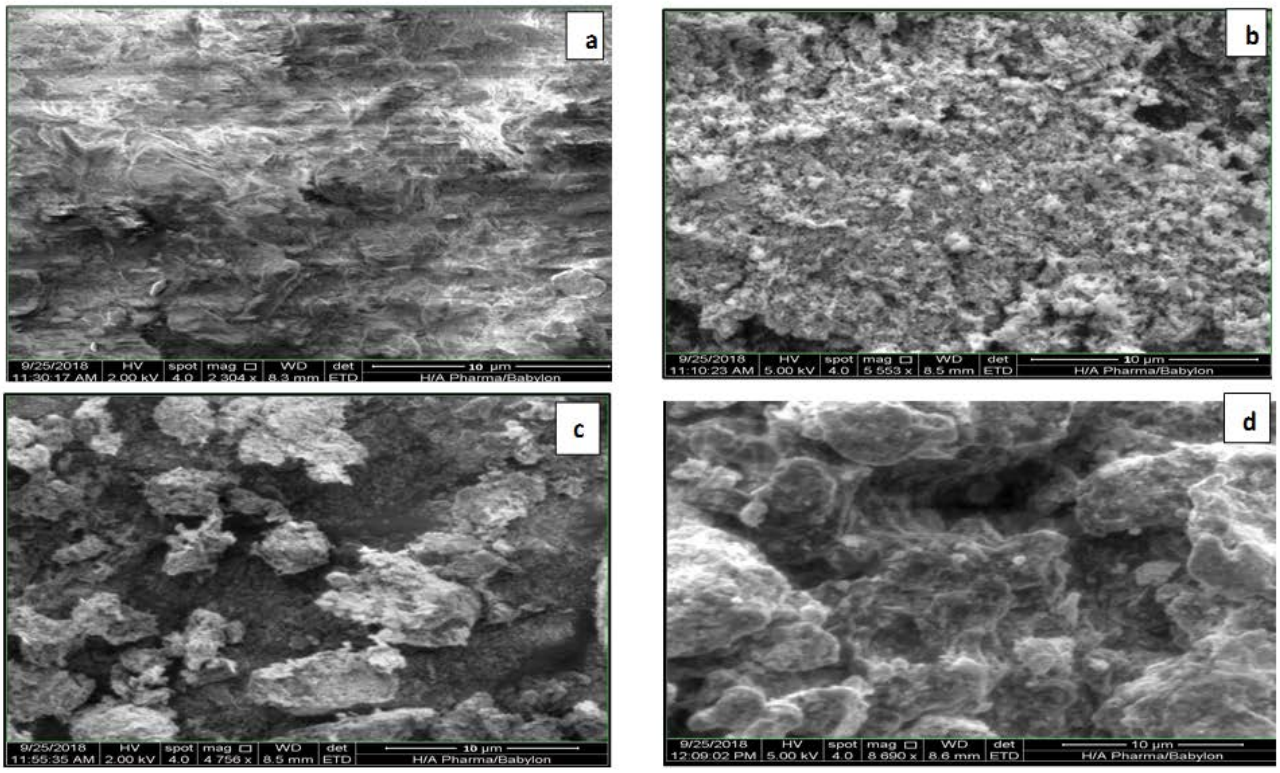

Fig. 5. SEM images for (a) PIS, (b) ZnO, and CPS (c) before and (d) after CIP adsorption.

aggregates are coalesced as pore surfaces were entirely filled with CIP molecules. This observation states that CIP were adsorbed onto the active surface groups that exist inside the pores and the well-formed pores on the CIP may be the main reason behind the high antibiotics uptake [22].

The FTIR spectroscopic analysis of the PIS and CPS before and after CIP adsorption is shown in Figs. 6a–c, in 500–4,000 cm^{-1} range. The analysis was used to show the existence of "surface functional groups" responsible for the CIP elimination procedure because these influence the achievement, govern adsorption mechanisms and solid adsorbent capacity since the adsorption process does not depend only on surface area [19].

The existence of fats in agriculture adsorbent is usually sensed by aliphatic C–H band (3,000–2,800 cm^{-1}), C=O band (1,745–1,725 cm^{-1}), carbohydrates (1,400–800 cm^{-1}) owing to bands between glucose polymers chains. PIS consists of four functionally important groups as displayed in Fig. 6a. The broad band detected at 3,414; 2,929.09; (1,500.62 and 1,384.00), and 894.97 cm^{-1} is assigned to O–H bond, C–H bond stretching, bonds between polymer chains, and benzene derivative vibrations, respectively. Fig. 6b displays the FTIR analysis of CPS; band at 563.21 cm^{-1} is related to inorganic ZnO stretching. Compared with the FTIR of PIS, there are clear shifts in CPS FTIR bands to novel values "3,410.15; 2,912.51; 1,427.32; 1,373.32; and 898.83 cm^{-1}", which owing to interactions between PIS and ZnONP. Also, the presence of band at 1,735.93 cm^{-1} is fit to ν(C=O) vibration in "carbonyl group or carboxylic bonds". The band at 1,604.77 cm^{-1} is recognized to the incidence of "C=O ring or C=C stretching of aromatic groups". The two bands absorption sensed at 1,330.88 and 1,045.02 cm^{-1} are matched to the stretching vibration of C–H and C–O groups of alcohol, separately show the FTIR of CPS after adsorption of CIP. The significant shifted peaks detected were 3,387.00; 2,908.00; 1,629.92; and 1,253.73 cm^{-1}, which are attributed to amine (N–H) band, carboxylic acid (O–H) band, quinones group (N–H) band, and (O–H) alcohol group, new peak appeared in 1,100 range, which is attributed to alkylhalide (C–F) band; these shifted and new peaks belong to adsorption of CIP on CPS [13,19,23].

3.2. Affecting parameters

The experiments were conducted to determine the effects of pH, CPS dose, particle size, shaking speed, temperature, initial CIP concentration, and time on the removal efficiency of CIP onto CPS; the results were illustrated in Figs. 7a–f. pH is an important factor on the adsorption efficiency, since the difference in the pH value produces changes in the CPS surface properties and CIP ionization state [18]. CPS point of zero charge was found to be 6.65, hence CPS may have positive (+) or negative (–) charge as solution has pH less or more than 6.5, respectively. The highest adsorption of CIP onto the CPS occurred at a pH of about 7 as shown in Fig. 7a; CIP as mentioned previously has two dissociation constants pKa_1 (for carboxylic acid group) = 6.1 and pKa_2 (for amine group) = 8.7. The cationic

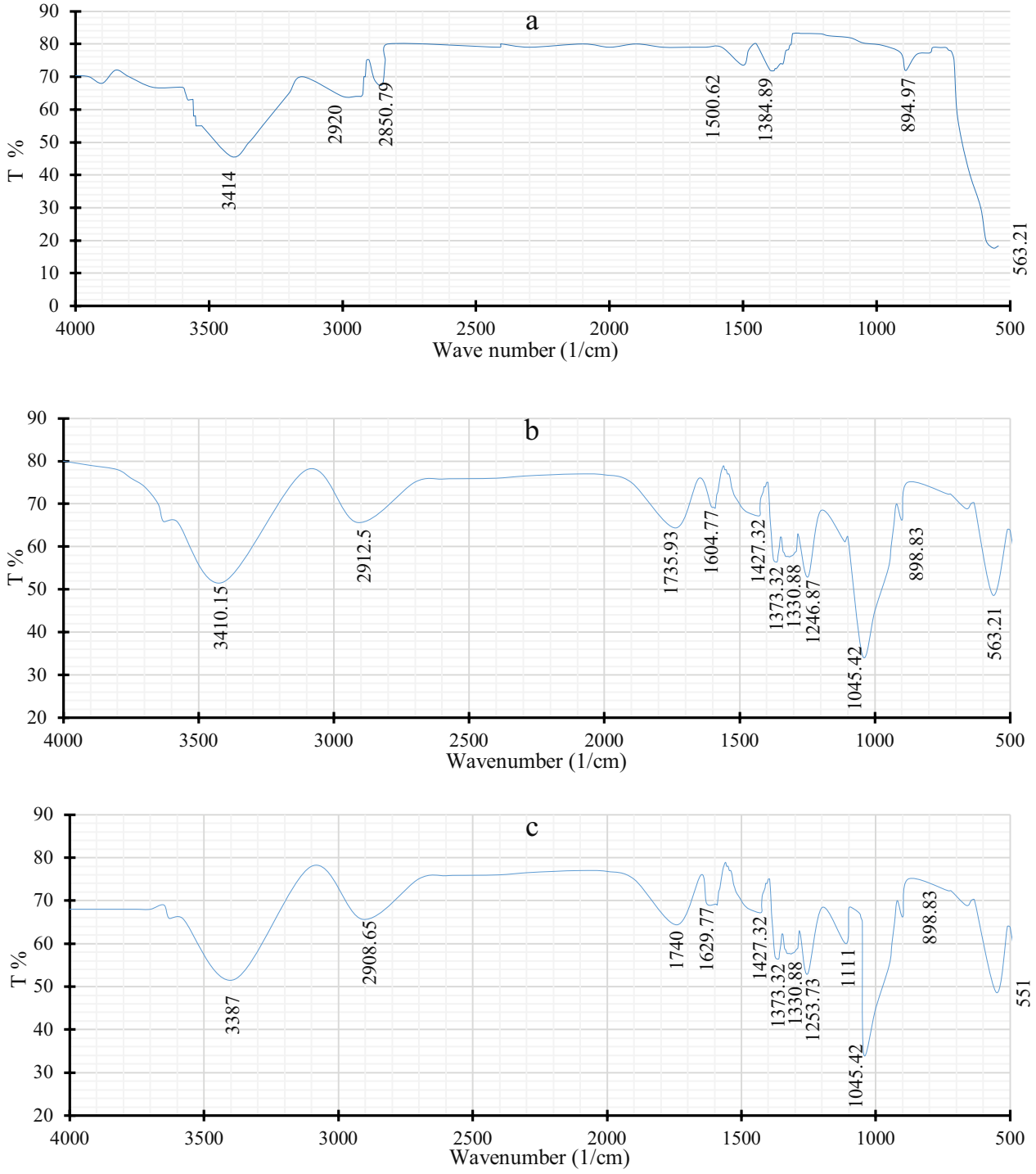

Fig. 6. FTIR analysis of (a) PIS, and CPS (b) before and (c) after CIP adsorption.

state present due to protonation of the amine group prevails at solution pH less than 6.1. Also, CIP zwitter ionic form exists at pH range (6.1–8.7). Maximum removal efficiency was 89.1% at pH 7. At the pH of 7, the zwitter ion form of CIP reaches its maximum percentage and this facilitates electrostatic attraction between negatively charged atoms of carboxyl groups within CIP and positively charged sites of the CPS adsorbents surface [14]. The adsorbent/solution ratio is a vital factor that influences the capacity of CPS and also the influence of sorbent doses on the CIP removal has been displayed in Fig. 7b. It represents the expected form of increasing adsorption as the adsorbent dose was increased. This is perhaps to mass transfer resistance of CIP from bulk solution to the CPS surface. It can be obviously seen that

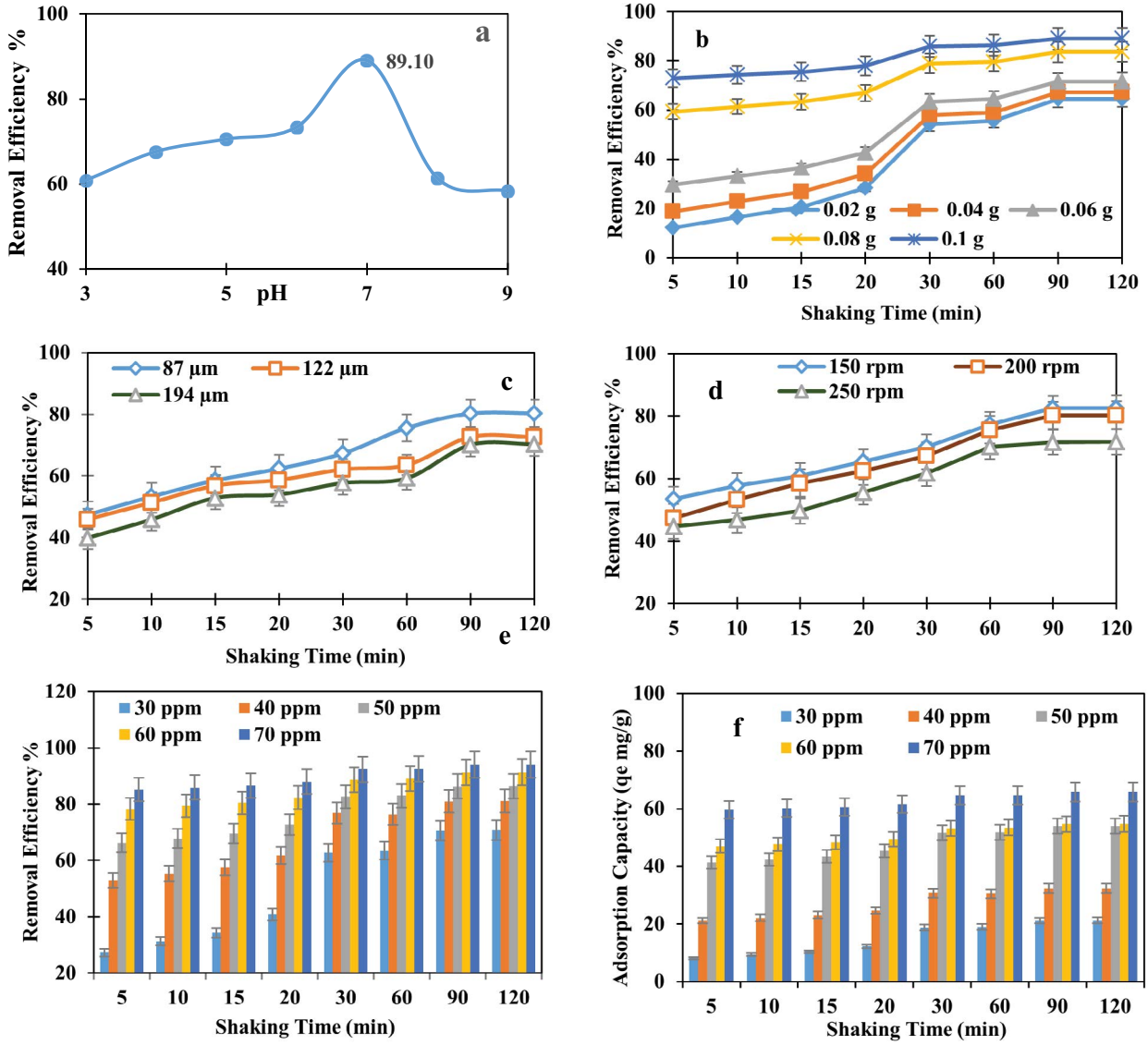

Fig. 7. Effect of experimental factors on CIP adsorption onto the CPS; pH (a), CPS dose (b), CPS particle size (c), shaking speed (d), adsorption uptake (e), and CIP initial concentration and contact time (f).

the elimination of CIP increased from 64.59% to 89.10% as the adsorbent dose increased from 0.02 to 0.1 g/100 mL CIP solution. As it can be predicted, at constant CIP initial concentration, increase in adsorbent dose increases the surface area that results in higher number of sorption places and therefore improvement in CIP uptake [24]. Depending on these consequences, 0.1 g/100 mL was chosen as the "best dose" for the following experiments. Fig. 7c displays the relationship between contact time and CIP elimination efficiency for various adsorbent particle sizes "194, 122, and 87 µm" at optimum pH and CPS dose obtained from the earlier experiments. The results display that the CIP elimination raised from 73.85% to 89.10% with a reduction in particle size from "194 to 87 µm". This observation clarifies the point that smaller particle sizes provide more surface area, which permit quick adsorption, and vice versa [25,26]. Mass transfer may be influenced by shaking speed [27] and to study the effect of changing the parameter on CIP adsorption, three values of speeds were investigated "150, 200, and 250 rpm" at pH, CPS dose, and particle size optimum value as shown in Fig. 7d. Removal efficiency decreased from 91.28% to 87.85% as shaking speed increased from 150 to 250 rpm. This is clear because kinetic energy of both CPS particles and CIP rises so much that collision starts, due to which weakly bounded molecules of CIP become detached from adsorbent particles [28]. Hence for further experiments, 150 rpm shaking speed was selected. To test the influence of CIP "initial concentration and contact time" on the adsorption behavior, CIP concentrations were differed from 30 to 70 mg/L under the best condition values obtained from the previous experiments. Fig. 7e illustrates the CIP elimination efficiency as a function of initial CIP concentration and time of contact. CIP elimination efficiency increased from 70.71% to 94.02% as initial CIP concentrations raised

from 30 to 70 mg/L. Elimination efficiency and adsorption uptake were rapid at the first 30 min. Then a small increase was noticed till adsorption attained equilibrium. The result investigates that adsorption occurs speedily at the first stage, that is, on the CPS external surface and then occurred at the internal through diffusion process, which may be the rate determining step [24]. Hence, the rapid adsorption at the early step possibly attributed to the point that a huge number of surface area exists for adsorption, but after time lapse the residual surface area will not be fully occupied easily by CIP molecules owing to the repulsion between the solid solute molecules and bulk phases, which spend long time to reach equilibrium [24]. Depending on these outcomes, a contact time of 90 min was chosen as the equilibrium time for the following experiments as equilibrium was attained at this period and higher adsorption was obtained. Fig. 7f shows that uptake capacity (q_e) at equilibrium increased from 21.21 to 65.82 mg/g with an increase in the CIP initial concentrations from 30 to 70 mg/L. This was owing to an escalation in concentration "driving force" with an increase in the CIP initial concentration [29].

3.3. Effect of temperature and thermodynamic analysis

The effect of solution temperature on the CIP removal efficiency was investigated and the results are plotted in Fig. 8. From this figure, it can be noticed that the removal efficiency decreased from 91.28% to 77.37% as the temperature increases from 25°C to 35°C due to an increase in the mobility of the adsorbate from the solid phase to the bulk phase. This causes adsorbent surface deactivation or the destruction of some active sites, hence desorption occurred instead of adsorption.

Thermodynamic parameters comprise [18] the following:

- $\Delta G°$: standard free energy change (kJ/mol; Eq. (4))
- $\Delta H°$: standard enthalpy change (kJ/mol; Eq. (5))
- $\Delta S°$: standard entropy change (kJ/mol K; Eq. (6))

$$\Delta G° = -RT\ln K_d \tag{4}$$

$$\ln K_d = \frac{\Delta S°}{R} - \frac{\Delta H°}{RT} \tag{5}$$

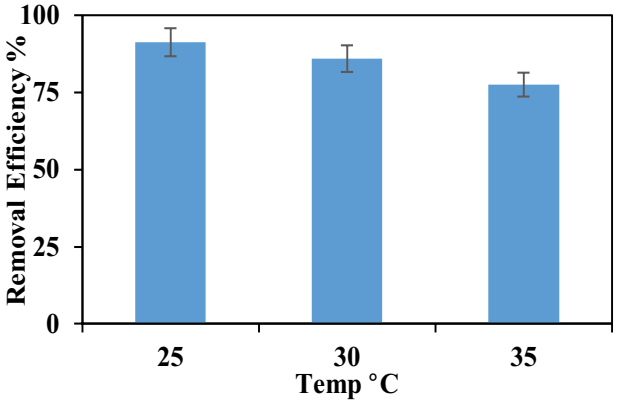

Fig. 8. Temperature changing effect on CIP adsorption onto CPS.

$$\Delta G° = \Delta H° - T\Delta S° \tag{6}$$

where R is the "universal gas constant" (8.314 J/mol K), T is the temperature (K), and K_d is the constant of equilibrium (q_e/C_e). These values were obtained from the intercept and slope of the plot of $\ln K_d$ vs. $1/T$, respectively. $\Delta H°$, $\Delta S°$, and $\Delta G°$ values are given in Table 2.

The negative value of $\Delta G°$ indicates that the CIP adsorption onto adsorbent used was spontaneous and feasible. The negative value of $\Delta H°$ indicates that the adsorption process of CIP was exothermic [18,30,31].

The $\Delta S°$ negative value showed a decrease in randomness at the solid/liquid boundary during the adsorption process. Enthalpy of adsorption usually either physical in $\Delta H°$ range (5–40 kJ/mol) or chemical in $\Delta H°$ range (40–800 kJ/mol): $\Delta H°$ value proposes CIP adsorption onto CPS as chemisorption [18,30,31].

3.4. Kinetic study

Mechanism of adsorption and rate-limiting steps specified by adsorption kinetics model included pseudo-first-order (PFO; Eq. (7) and Fig. 9a) [32] and pseudo-second-order (PSO; Eq. (8) and Fig. 9b) [32].

$$\ln\left(q_e - q_t\right) = \ln q_e - k_1 t \tag{7}$$

$$\frac{t}{q_t} = \frac{1}{k_2 q_e} + \frac{t}{q_e} \tag{8}$$

where q_e and q_t (mg/g) are the quantity of CIP adsorbed at equilibrium and at any time t, respectively, k_1 (min^{-1}) and k_2 (g/mg min) are the PFO and the PSO constants, respectively. The preliminary adsorption rate h (mg/g min) can be calculated from the PSO model at $t \to 0$ by Eq. (9) and Fig. 9b [18].

$$h = k_2 q_e \tag{9}$$

The kinetic parameters and correlation coefficients (R^2) achieved from the drawing linearized kinetic of PFO "t vs. $\ln(q_t - q_e)$" and PSO "t vs. t/q_t" are shown in Figs. 9a and b, and Table 2. By comparing R^2 and the agreement between the calculated q_e and the experimental q_e values of kinetic models applied, it was concluded that PSO kinetic model is more suitable to describe CIP adsorption behavior onto the CPS adsorbent since the R^2 values of PSO are higher than the R^2 values of PFO model and the difference in $q_{e,\text{cal}}$ and $q_{e,\text{exp}}$ are small; k_2 values reduce with an increase in initial CIP concentrations and surface

Table 2
Thermodynamic parameters of CIP adsorption onto CPS

Temp. (K)	$\Delta G°$ (kJ/mol)	$\Delta H°$ (kJ/mol)	$\Delta S°$ (kJ/mol K)
298	–5,861.166		
303	–4,516.001	–86.033272	–269.033
308	–3,170.836		

loading [33]. Mechanisms of diffusion cannot be recognized from the mentioned kinetic models. The "intraparticle diffusion" (Ipd) model was clarified by Eq. (10) [34] below:

$$q_t = k_{id} t^{0.5} + C \tag{10}$$

where k_{id} (mg/g min$^{1/2}$) is the constant of intraparticle rate and C (mg/g) is indicative of thickness of boundary layer. C value close to zero states that diffusion is the only guiding method in the adsorption process [25]. If the scheme of q_t vs. $t^{1/2}$ as illustrated in Fig. 9c is a straight line, intraparticle diffusion is the adsorption mechanism. Hence, k_{id} and C can be obtained from the slope and intercept of the draw, respectively. On the other hand, intraparticle diffusion schemes were not linear with time, which point to CIP adsorption onto CPS was guided by different mode of adsorption. The plot above does not pass over the point of origin, which indicates that intraparticle diffusion was existent not as the only rate controlling step but some additional mechanisms have also been included. The values of k_{id} and C are shown in Table 3. From this table, it can be noticed that with an increase in CIP initial concentration, k_{id} values increased. This may enhance the driving force with increasing CIP initial concentration. This fact proved that the boundary layer diffusion is the rate-limiting step not intraparticle diffusion [34].

3.5. Isotherm study

The adsorption isotherm is a graphical illustration of quantity of material adsorbed vs. the remaining solution adsorbate concentration [24]. The adsorption data for CIP concentration and CPS doses were examined using Freundlich and Langmuir isotherms to find the adsorption capability of CIP by applied Eqs. (11) and (12) [35].

$$q_e = K_F C_e^{1/n} \tag{11}$$

$$q_e = \frac{q_m K_L C_e}{1 + K_L C_e} \tag{12}$$

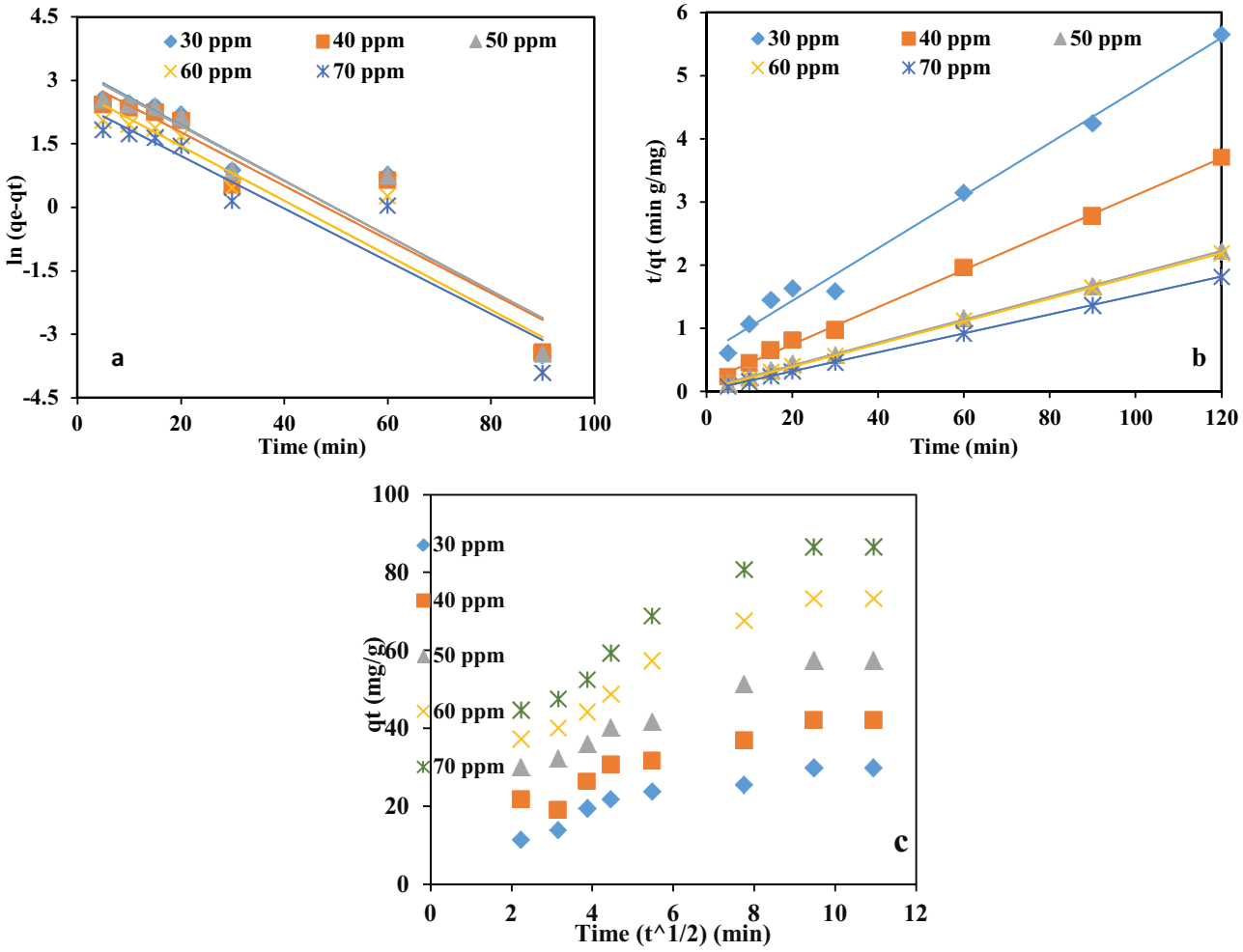

Fig. 9. Time-dependent adsorption efficiency of CPS for CIP corresponding to (a) pseudo-first-order, (b) pseudo-second-order, and (c) Ipd adsorption kinetic models.

Table 3
Kinetic data for the CIP adsorption on CPS at different initial concentrations

Model		PFO			PSO				Ipd		
C_0	$q_{e,exp}$ (mg/g)	$q_{e,cal}$ (mg/g)	k_1 (1/min)	R^2	$q_{e,cal}$ (mg/g)	k_2 (g/mg min)	R^2	h (mg/g min)	k_{id} (m/g min$^{1/2}$)	C (mg/g)	R^2
30	21.21	10.35	0.0571	0.8963	21.88	0.01202	0.99	5.76	0.7713	13.815	0.839
40	32.42	12.94	0.056	0.8523	33.11	0.01001	0.9993	10.98	0.8132	24.217	0.9498
50	54.00	15.02	0.0576	0.8482	54.64	0.00960	0.9997	28.65	0.9232	44.712	0.9453
60	54.77	17.86	0.0621	0.8127	54.64	0.00962	0.9995	28.74	1.0103	44.587	0.9269
70	65.82	21.70	0.0693	0.9338	66.23	0.00838	0.9999	36.76	1.3012	53.415	0.8795

PFO: pseudo-first-order; PSO: pseudo-second-order; Ipd: intraparticle diffusion.

where K_F: the Freundlich constant concerning to the adsorption capacity q_e (mg/g); n: the heterogeneity factor (g/L); q_m: maximum adsorption capacity (mg/g); K_L: Langmuir constant linked to the tendency between the adsorbate and adsorbent (L/mg).

Here, models parameters were determined by "nonlinear regression analysis" by using solver tool in Microsoft excel. Isotherm model effectiveness with the experimental equilibrium records was detected by the determination coefficient values (R^2) as shown in Table 4 and Fig. 10 [35,36].

Hence to describe this, the R_L "dimensionless equilibrium constant" will be determined by using Eq. (13):

$$R_L = \frac{1}{1 + K_L C_0} \tag{13}$$

where C_o: initial CIP concentration (mg/L).

If $R_L > 1$ describes unfavorable, $0 < R_L < 1$ describes favorable, $R_L = 1$ illustrates linear and $R_L = 0$ characterizes the irreversible characteristics of the process [18].

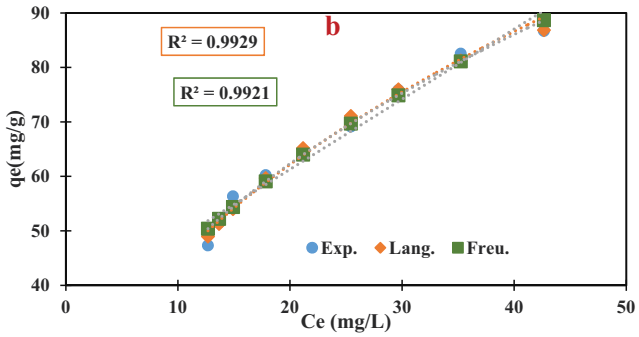

Fig. 10. Isotherm data of CIP adsorption onto the CPS.

The results above show that R^2 values of Langmuir and Freundlich models are close to each other and to unity and hence it can be said that two models are compatible. SSE, for Langmuir model were less than Freundlich model, then the adsorption occurs under homogeneous and monolayer surfaces with the maximum adsorption capacity of 129.1 mg/g for CIP. Whether the adsorption is favorable at the examined conditions can be evaluated based on the two aforementioned criteria: adsorption intensity parameter (n) and separation factor (R_L), derived from the Freundlich and Langmuir models, respectively. Values of n greater than unity indicates a favorable adsorption taking place, and R_L values lower than 1 implies favorable adsorption occurring.

4. Conclusions

"Pistachio shells coated with ZnO nanoparticles (CPS)" were produced and applied for elimination of CIP from simulated wastewater. Consequences display that the adsorption of CIP on the CPS adsorbents is intensely pH dependent. Langmuir model was found to be best fitted than Freundlich model with maximum uptake at 129.1 mg/g. The kinetic data were modeled and the adsorption trend was observed to obey the pseudo-second-order kinetic model indicating the chemisorption mechanism onto CPS and intraparticle diffusion was active but it is not the only rate controlling step, and another mechanism can be associated. C values were greater than zero and increased with initial antibiotics concentration increasing confirming that adsorption process rate limiting contributes to the diffusion of the boundary layer, not intraparticular diffusion. In conclusion, the thermodynamic study displayed exothermic CIP adsorption. The results point that CPS is an excellent media for CIP elimination and can be utilized in the adsorption method for the elimination of CIP from aqueous solutions.

Table 4
Isotherm model parameters of CIP adsorption onto CPS

Freundlich				Langmuir				
K_f	n	R^2	SSE	q_m (mg/g)	K_L	R^2	R_L	SSE
15.45	2.14	0.9921	22.85	129.1	0.048	0.9929	0.25	14.29

References

[1] H. Chen, B. Gao, H. Li, L.Q. Ma, Effects of pH and ionic strength on sulfamethoxazole and ciprofloxacin transport in saturated porous media, J. Contam. Hydrol., 126 (2011) 29–36.

[2] V. Homem, L. Santos, Degradation and removal methods of antibiotics from aqueous matrices – a review, J. Environ. Manage., 92 (2011) 2304–2347.

[3] H. Nakata, K. Kannan, P.D. Jones, J.P. Giesy, Determination of fluoroquinolone antibiotics in wastewater effluents by liquid chromatography-mass spectrometry and fluorescence detection, Chemosphere, 58 (2005) 759–766.

[4] C.-J. Wang, Z.H. Li, W.-T. Jiang, Adsorption of ciprofloxacin on 2:1 dioctahedral clay minerals, Appl. Clay Sci., 53 (2011) 723–728.

[5] M. Ashfaq, K. Nawaz Khan, M. Saif Ur Rehman, G. Mustafa, M. Faizan Nazar, Q. Sun, J. Iqbal, S.I. Mulla, C.-P. Yu, Ecological risk assessment of pharmaceuticals in the receiving environment of pharmaceutical wastewater in Pakistan, Ecotoxicol. Environ. Saf., 136 (2017) 31–39.

[6] M. Al-Saraj, M.S. Abdel-Latif, I. El-Nahal, R. Barak, Bioaccumulation of some hazardous metals by sol–gel entrapped microorganisms, J. Non-Cryst. Solids, 248 (1999) 137–140.

[7] D.T. Ajeel Al-Heetimi, M.A.R. Kadhum, O.S. Alkhazrajy, Adsorption of ciprofloxacin hydrochloride from aqueous solution by Iraqi porcelinaite adsorbent, J. Al-Nahrain Univ., 17 (2014) 41–49.

[8] N. Dhiman, N. Sharma, Batch adsorption studies on the removal of ciprofloxacin hydrochloride from aqueous solution using ZnO nanoparticles and groundnut (*Arachis hypogaea*) shell powder: a comparison, Ind. Chem. Eng., 61 (2019) 67–76.

[9] S.H. Siddiqui, R. Ahmad, Pistachio shell carbon (PSC) – an agricultural adsorbent for the removal of Pb(II) from aqueous solution, Groundwater Sustainable Dev., 4 (2017) 42–48.

[10] N. Genç, Removal of antibiotic ciprofloxacin hydrochloride from water by kandira stone: kinetic models and thermodynamic, Global Nest J., 17 (2015) 498–507.

[11] S. Neeta, D. Neha, Kinetic and thermodynamic studies for ciprofloxacin hydrochloride adsorption from aqueous solution on Cuo nanoparticles, Int. J. ChemTech Res., 10 (2017) 98–106.

[12] F. Yu, S. Sun, S. Han, J. Zheng, J. Ma, Adsorption removal of ciprofloxacin by multi-walled carbon nanotubes with different oxygen contents from aqueous solutions, J. Mol. Liq., 285 (2016) 588–595.

[13] M. Gilani, S. Zahra, Adsorption of Ciprofloxacin from Water by Adsorbents Developed from Oat Hulls, Master's Thesis, University of Saskatchewan, Saskatoon, 2018.

[14] V. Pifferi, G. Cappelletti, S. Ardizzone, L. Falciola, C. Di Bari, F. Spadavecchia, D. Meroni, A. Carrà, G. Cerrato, S. Morandi, E. Davoli,. Photo-mineralization of noxious *o*-toluidine water pollutant by nano-ZnO: the role of the oxide surface texture on the kinetic path, Appl. Catal., B, 178 (2015) 233–240.

[15] H. Moussa, E. Girot, K. Mozet, H. Alem, G. Medjahdi, R. Schneider, ZnO rods/reduced graphene oxide composites prepared *via* a solvothermal reaction for efficient sunlight-driven photocatalysis, Appl. Catal., B, 185 (2016) 11–21.

[16] Y.P. Zhao, J.J. Geng, X.R. Wang, X.Y. Gu, S.X. Gao, Adsorption of tetracycline onto goethite in the presence of metal cations and humic substances, J. Colloid Interface Sci., 361 (2011) 247–251.

[17] M.M. Soori, E. Ghahramani, H. Kazemian, T.J. Al-Musawi, M. Zarrabi, Intercalation of tetracycline in nano sheet layered double hydroxide: an insight into UV/VIS spectra analysis, J. Taiwan Inst. Chem. Eng., 63 (2016) 271–285.

[18] A.A. Mohammed, Biosorption of lead, cadmium, and zinc onto sunflower shell: equilibrium, kinetic, and thermodynamic studies, Iraqi. J. Chem. Petrol. Eng., 16 (2015) 91–105.

[19] S. Sharma, Neeraj, FTIR spectroscopic characterization of almond varieties (*Prunus dulcis*) from Himachal Pradesh (India), Int. J. Curr. Microbiol. Appl. Sci., 7 (2018) 887–898.

[20] A.C. Lua, T. Yang, Characteristics of activated carbon prepared from pistachio-nut shell by zinc chloride activation under nitrogen and vacuum conditions, J. Colloid Interface Sci., 290 (2005) 505–513.

[21] M. Ersana, U.A. Guler, U. Acıkel, M. Sarioglu, Synthesis of hydroxyapatite/clay and hydroxyapatite/pumice composites for tetracycline removal from aqueous solutions, Process Saf. Environ. Prot., 96 (2015) 22–32.

[22] P.-H. Chang, Z.H. Li, T.-L. Yu, S. Munkhbayer, T.-H. Kuo, Y.-C. Hung, J.-S. Jean, K.-H. Lin, Sorptive removal of tetracycline from water by palygorskite, J. Hazard. Mater., 165 (2009) 148–155.

[23] A.A. Mohammed, T.J. Al-Musawi, S.L. Kareem, M. Zarrabi, A.M. Al-Ma'abreh, Simultaneous adsorption of tetracycline, amoxicillin, and ciprofloxacin by pistachio shell powder coated with zinc oxide nanoparticles, Arabian J. Chem., 13 (2020) 4629–4643.

[24] A.M.K. Aljebori, A.N. Alshirifi, Effect of different parameters on the adsorption of textile dye maxilon blue grl from aqueous solution by using white marble, Asian J. Chem., 24 (2012) 5813–5816.

[25] K.K.I.U. Arunakumara, B.C. Walpola, M.-H. Yoon, Banana peel: a green solution for metal removal from contaminated water, Korean J. Environ. Agric., 32 (2013) 108–116.

[26] A.A. Mohammed, S.L. Kareem, Adsorption of tetracycline fom wastewater by using Pistachio shell coated with ZnO nanoparticles: equilibrium, kinetic and isotherm studies, Alexandria Eng. J., 58 (2019) 917–928.

[27] K. Vijayaraghavan, Y.-S. Yun, Bacterial biosorbents and biosorption, Biotechnol. Adv., 26 (2008) 266–291.

[28] S. Arivoli, M. Henkuzhali, Kinetic, mechanistic, thermodynamic and equilibrium studies on the adsorption of rhodamine b by acid activated low cost carbon, E-J. Chem., 5 (2008) 437375, https://doi.org/10.1155/2008/437375.

[29] H. Sayğılı, F. Güzel, Effective removal of tetracycline from aqueous solution using activated carbon prepared from tomato (*Lycopersicon esculentum* Mill.) industrial processing waste, Ecotoxicol. Environ. Saf., 131 (2016) 22–29.

[30] J. Gülen, F. Zorbay, Methylene blue adsorption on a low cost adsorbent-carbonized peanut shell, Water Environ. Res., 89 (2017) 805–816.

[31] J. Gülen, M. İskeçeli, Removal of methylene blue by using porous carbon adsorbent prepared from carbonized chestnut shell, Mater. Test., 59 (2017) 188–194.

[32] J. Gülen, S. Aslan, Adsorption of 2,4-dichlorophenoxyacetic acid from aqueous solution using carbonized chest nut as low cost adsorbent: kinetic and thermodynamic, Z. Phys. Chem., 234 (2020) 461–484.

[33] W.J. Weber, J.C. Morris, Kinetics of adsorption on carbon from solution, J Sanitary Eng. Div. Am. Soc. Civ. Eng., 89 (1963) 31–60.

[34] S.H. Chen, J. Zhang, C.L. Zhang, Q.Y. Yue, Y. Li, C. Li, Equilibrium and kinetic studies of methyl orange and methyl violet adsorption on activated carbon derived from *Phragmites australis*, Desalination, 252 (2010) 149–156.

[35] S. Azizian, M. Bagheri, Enhanced adsorption of Cu^{2+} from aqueous solution by Ag doped nano-structured ZnO, J. Mol. Liq., 196 (2014) 198–203.

[36] B.J. Zhang, J.W. Ji, X. Liu, C.S. Li, M. Yuan, J.Y. Yu, Y.Q. Ma, Rapid adsorption and enhanced removal of emodin and physcion by nano zirconium carbide, Sci. Total Environ., 647 (2019) 57–65.